Fast Vesicle Fusion in Living Cells Requires at Least Three SNARE Complexes

Ralf Mohrmann, *et al.*

Science **330**, 502 (2010);
DOI: 10.1126/science.1193134

hyperactivated *NP394-neurons* showed promoted light avoidance, we propose that *NP394-neuron* activity is positively correlated with larval light-avoidance ability. Two possible scenarios could be operating in this situation. First, the activity of *NP394-neurons* itself controls the larval phototaxis by an unknown mechanism. Second, the *NP394-neurons* activate the pathway that mediates avoidance of light whereas other unidentified neurons activate the pathway that underlies avoidance of darkness, as was shown for the mechanisms underlying odor-taxis in adult *Drosophila* (*25*).

References and Notes

1. J. N. Crawley, *What's Wrong With My Mouse? Behavioral Phenotyping of Transgenic and Knockout Mice* (Wiley, New York, 2000).
2. M. Manning, T. A. Markow, *Behav. Genet.* **11**, 557 (1981).
3. J. Grossfield, *Proc. Natl. Acad. Sci. U.S.A.* **68**, 2669 (1971).
4. Y. Ben-Shahar, H. T. Leung, W. L. Pak, M. B. Sokolowski, G. E. Robinson, *J. Exp. Biol.* **206**, 2507 (2003).
5. F. P. Sawin, L. R. Harris, A. R. Campos, M. B. Sokolowski, *J. Insect Behav.* **7**, 553 (1994).
6. E. O. Mazzoni, C. Desplan, J. Blau, *Neuron* **45**, 293 (2005).
7. E. P. Sawin-McCormack, M. B. Sokolowski, A. R. Campos, *J. Neurogenet.* **10**, 119 (1995).
8. C. Helfrich-Förster *et al.*, *J. Neurosci.* **22**, 9255 (2002).
9. S. G. Sprecher, C. Desplan, *Nature* **454**, 533 (2008).
10. S. Malpel, A. Klarsfeld, F. Rouyer, *Development* **129**, 1443 (2002).
11. J. Hassan, B. Iyengar, N. Scantlebury, V. Rodriguez Moncalvo, A. R. Campos, *J. Comp. Neurol.* **481**, 266 (2005).
12. M. Busto, B. Iyengar, A. R. Campos, *J. Neurosci.* **19**, 3337 (1999).
13. S. T. Sweeney, K. Broadie, J. Keane, H. Niemann, C. J. O'Kane, *Neuron* **14**, 341 (1995).
14. M. N. Nitabach, J. Blau, T. C. Holmes, *Cell* **109**, 485 (2002).
15. A. M. van der Bliek, E. M. Meyerowitz, *Nature* **351**, 411 (1991).
16. M. N. Nitabach *et al.*, *J. Neurosci.* **26**, 479 (2006).
17. C. H. Yang *et al.*, *Neuron* **61**, 519 (2009).
18. H. Dircksen *et al.*, *Cell Tissue Res.* **250**, 377 (1987).
19. W. Li *et al.*, *Cell Tissue Res.* **336**, 509 (2009).
20. J. Wang *et al.*, *Neuron* **43**, 663 (2004).
21. E. H. Feinberg *et al.*, *Neuron* **57**, 353 (2008).
22. M. D. Gordon, K. Scott, *Neuron* **61**, 373 (2009).
23. Y. Shang, L. C. Griffith, M. Rosbash, *Proc. Natl. Acad. Sci. U.S.A.* **105**, 19587 (2008).
24. L. Tian *et al.*, *Nat. Methods* **6**, 875 (2009).
25. J. L. Semmelhack, J. W. Wang, *Nature* **459**, 218 (2009).

26. We thank K. Rao for antibody to Pdf; J. Blau, K. Scott, M. Rosbach, T. Lee, C. Feng, Y. Zhong, W. Yi, Y. Jan, and R. Jiao for fly stocks and constructs; and C. Wang and X. Hao for facility setup. We thank the DGRC (Kyoto) and the Bloomington fly stock center for the fly stocks, and Developmental Studies Hybridoma Bank for antibodies. We also thank H. Gong for technical assistance, and J. Fleming and R. Wolf for valuable comments. This work was supported by the National Natural Sciences Foundation of China [grant 30770682 (Z.G.) and grants 30621004 and 30625022 (L.L.)], the '973 Program' [grants 2005CB522804 and 2009CB918702 (L.L.)], and the Knowledge Innovation Program of the Chinese Academy of Sciences [grant KSCX2-YW-R-247 (L.L.)].

Supporting Online Material

www.sciencemag.org/cgi/content/full/330/6003/499/DC1
Materials and Methods
Figs. S1 to S13
Table S1
References
Movies S1 to S3

3 August 2010; accepted 8 September 2010
10.1126/science.1195993

Fast Vesicle Fusion in Living Cells Requires at Least Three SNARE Complexes

Ralf Mohrmann,[1,2]* Heidi de Wit,[3] Matthijs Verhage,[3] Erwin Neher,[1] Jakob B. Sørensen[1,4,5]*

Exocytosis requires formation of SNARE [soluble *N*-ethylmaleimide–sensitive factor attachment protein (SNAP) receptor] complexes between vesicle and target membranes. Recent assessments in reduced model systems have produced divergent estimates of the number of SNARE complexes needed for fusion. Here, we used a titration approach to answer this question in intact, cultured chromaffin cells. Simultaneous expression of wild-type SNAP-25 and a mutant unable to support exocytosis progressively altered fusion kinetics and fusion-pore opening, indicating that both proteins assemble into heteromeric fusion complexes. Expressing different wild-type:mutant ratios revealed a third-power relation for fast (synchronous) fusion and a near-linear relation for overall release. Thus, fast fusion typically observed in synapses and neurosecretory cells requires at least three functional SNARE complexes, whereas slower release might occur with fewer complexes. Heterogeneity in SNARE-complex number may explain heterogeneity in vesicular release probability.

The SNARE [soluble *N*-ethylmaleimide–sensitive factor attachment protein (SNAP) receptor] complex formed between two fusing membranes is at the heart of the molecular machinery that mediates exocytosis (*1*). It is a coiled bundle of four parallel α helices provided by three SNARE proteins: SNAP-25 (synaptosome-associated protein of 25 kD), synaptobrevin-2, and syntaxin-1 (*2*). SNARE-complex formation proceeds from the N- to the C-terminal end in a discontinuous process that involves partially assembled intermediates. Assembly of the most C-terminal three to four interaction layers coincides with membrane merger (*3*). Though it has been unclear whether assembly of one SNARE complex generates sufficient energy to initiate vesicle fusion (*4*–*7*), it was recently reported that liposomes can fuse with the help of a single SNARE complex, albeit with low speed (*8*). Other studies have concluded that 5 to 11 SNARE complexes might be involved in faster modes of fusion (*9*–*13*).

To study the dependence of fast vesicle fusion on higher-order SNARE complexes in intact cells, we used an exceptionally inhibitory SNAP-25 mutation in a titration assay that allowed us to relate exocytosis to the relative expression levels of mutant and wild-type (WT) protein in a given cell. Our mutant harbored two alanine substitutions [$Met^{71} \rightarrow Ala^{71}$ (M71A) and $Ile^{92} \rightarrow Ala^{92}$ (I192A)] in the interaction layer +5, facing the inside of the complex (*2*). If incorporated in the SNAP-25A isoform, this mutation completely fails to reconstitute exocytosis in *Snap-25*$^{-/-}$ adrenal chromaffin cells (*14*). Here, we introduced the mutation into SNAP-25B, because this isoform supports two to three times more fast-phase secretion (*15*). SNAP-25B WT (SN25B) or mutant protein (denoted SN25BL5**) were N-terminally fused to enhanced green fluorescent protein (EGFP) or mCherry (mCh), allowing for the quantitative analysis of expression levels and protein localization.

Using the Semliki Forest virus (SFV) expression system, we characterized mCh-tagged SN25BL5** and mCh-SN25B expressed separately in SNAP-25–deficient chromaffin cells (*16*). Both proteins were localized to the plasma membrane and expressed to similar levels (Fig. 1, E and F). Secretion was assayed by membrane capacitance measurements and amperometry after flash photorelease of caged calcium. Expression of mCh-SN25BL5** suppressed secretion (total capacitance change: 12 ± 3 fF after 5 s; $n = 28$ cells) (Fig. 1, A to E) compared with mCh-SN25B–infected cells (510 ± 54 fF; $n = 36$; $P < 0.0001$) and even SNAP-25–deficient cells (39 ± 5 fF; $n = 35$; $P < 0.0001$; Student's t test). This made SN25BL5** an attractive inhibitor for a titration experiment. Several lines of evidence indicate that inhibition probably arises from interference with a very late step of exocytosis associated with the C-terminal assembly of the SNARE complex: (i) SN25L5** forms stable SNARE complexes

[1]Department of Membrane Biophysics, Max-Planck Institute for Biophysical Chemistry, Göttingen, Germany. [2]Department of Physiology, University of Saarland, Homburg, Germany. [3]Center for Neurogenomics and Cognitive Research, Department of Functional Genomics, Vrije Universiteit (VU) Amsterdam and VU Medical Center, Amsterdam, Netherlands. [4]Department of Neuroscience and Pharmacology, Faculty of Health Sciences, University of Copenhagen, Copenhagen, Denmark. [5]Lundbeck Foundation Center for Biomembranes in Nanomedicine, University of Copenhagen, Copenhagen, Denmark.

*To whom correspondence should be addressed. E-mail: Ralf.Mohrmann@uks.eu (R.M.); jakobbs@sund.ku.dk (J.B.S.)

in vitro, exhibiting assembly kinetics indistinguishable from WT protein (*14*). However, mutant SNARE complexes exhibit a strongly destabilized C-terminal end (*14*). (ii) SNAP-25 is required for vesicle docking (*17*) before participating in downstream steps of exocytosis. Expression of SN25BL5** completely restored docking in *Snap-25*$^{-/-}$ cells (Fig. 1, G to I, and fig. S1), excluding an involvement of layer +5 in these early steps of exocytosis. (iii) The phenotypes caused by single point mutations in layer +5 of SN25B (M71A or I192A) indicate that assembly of this layer is important for fusion triggering. Expression of either mutant in *Snap-25*$^{-/-}$ cells slowed down fusion kinetics (fig. S2, A and B), similar to other mutations compromising the C-terminal end of the SNARE complex (*14*, *18*). In contrast, unchanged sustained-release rates (fig. S2Ab and S2Bb) and normal recovery between stimulations (fig. S2Ae and S2Be) suggest normal vesicle priming.

To obtain cells with varying ratios of mCh-SN25BL5** and EGFP-SN25B, we generated viruses harboring bicistronic expression units containing different "internal ribosome entry site" (IRES)–sequences (fig. S3) (*16*). After calibration with an EGFP-mCh fusion protein (fig. S3B), relative expression levels of the two fusion proteins were assessed by quantifying mCh and EGFP fluorescence. All viruses displayed substantial variations of expression ratios in individual cells, which were exploited to cover a wider range of expression ratios. The two fusion proteins colocalized closely (fig. S4), both on the plasma membrane and on certain intracellular structures (*19*).

In control recordings, EGFP-SN25B–expressing cells exhibited an average total capacitance increase of 483 ± 25 fF (n = 125). Progressively increasing fractional mCh-SN25BL5** expression

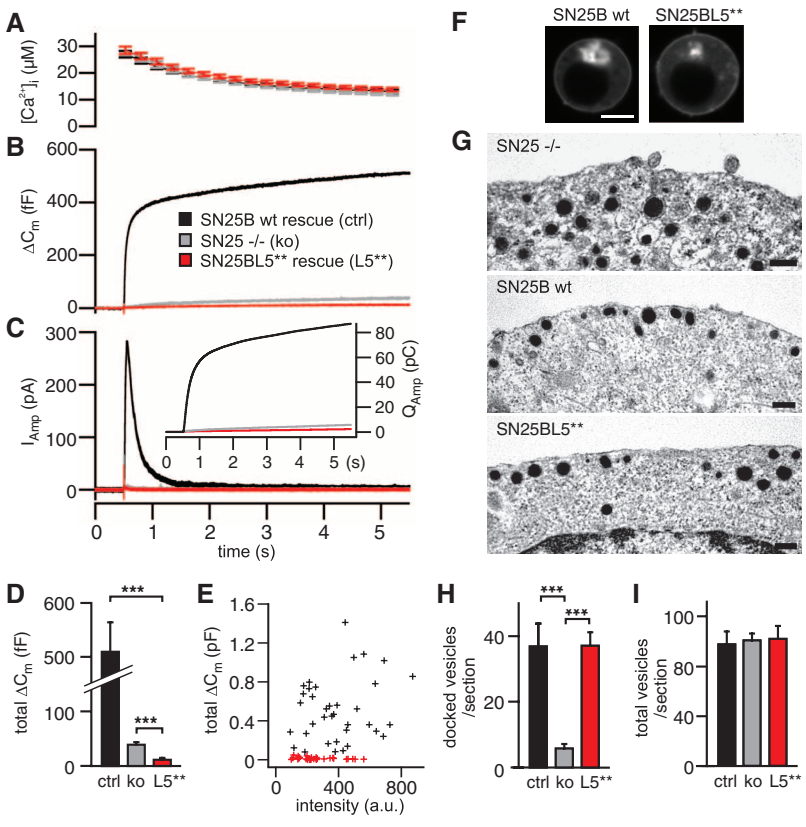

Fig. 1. A SNAP-25B mutant causes complete arrest of neurotransmitter release. (**A** to **C**) Averaged data for calcium uncaging experiments in *Snap-25*–deficient chromaffin cells (ko, knockout) (gray), knockout cells expressing mCh-SN25B wild type (ctrl) (black), or mCh-SN25B M71A, I192A (SN25BL5**; L5**) (red). (A) Intracellular calcium concentrations (mean ± SEM) after ultraviolet flash applied at 0.5 s. $[Ca^{2+}]_i$, intracellular concentration of Ca^{2+}. (B) Induced membrane capacitance change (ΔC_m). (C) Amperometric current (I_{Amp}). (Inset) Cumulative amperometric charge (Q_{Amp}). (**D**) Total capacitance change (mean ± SEM) reached after 5 s was significantly (***$P < 0.0001$, Student's t test) decreased by expression of SN25BL5**. (**E**) Plot of total capacitance change versus cellular fluorescence intensity. a.u., arbitrary units. (**F**) Confocal microphotographs of chromaffin cells expressing mCh-SN25B or mCh-SN25BL5**. Scale bar, 5 μm. (**G**) Sample electron micrographs of *Snap-25* knockout cell and knockout cell expressing WT SN25B or SN25BL5**. Scale bars, 200 nm. (**H**) Number of docked vesicles and (**I**) total number of vesicles (mean ± SEM) in *Snap-25* knockout cells and after rescue with SN25BL5** and WT protein (***$P < 0.001$).

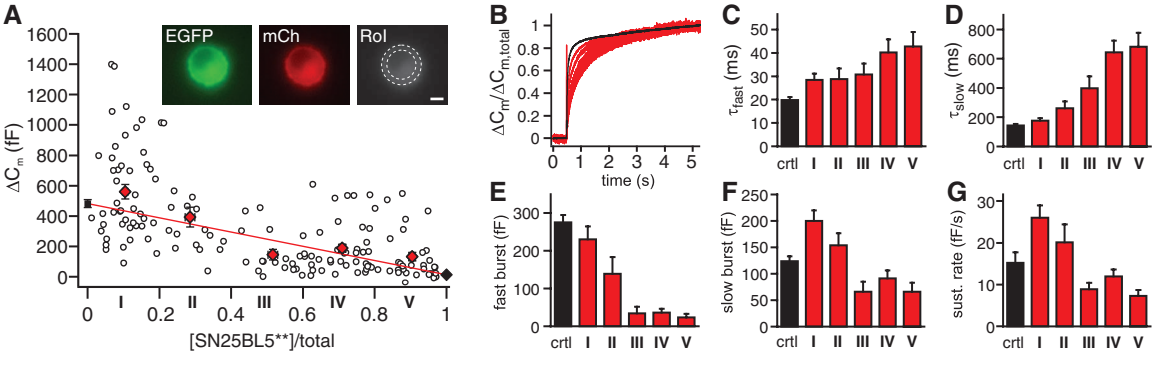

Fig. 2. Coexpression of SN25L5** with WT SNAP-25 is accompanied by a pronounced slowdown of release. (**A**) Plot of the overall capacitance change (5 s after flash) versus the fraction of mutant SNAP-25 expressed. Open circles represent single recordings; red diamonds denote mean data for five (I to V) binned groups; black symbols represent the capacitance change in cells expressing only EGFP-SN25B (0%) or mCh-SN25BL5** (100%). The red line indicates a strict linear relation between a fraction of SN25BL5** and inhibition, assuming no cooperativity. Error bars represent SEM. (Inset) Microphotographs of a chromaffin cell expressing both SNAP-25 variants. Fluorescence intensity was measured in a region of interest (RoI) enclosing the plasma membrane. Scale bar, 5 μm. (**B** to **D**) Kinetic analysis of capacitance changes. (B) Capacitance traces were averaged in each binned group (I to V, red; EGFP-SN25B, black) and normalized to their amplitude at 5 s. (C) Fast and (D) slow bursts show gradually increasing time constants (τ_{fast} and τ_{slow}, respectively) during titration with SN25BL5**. (**E**) The amplitude of the fast burst steadily decreases during the titration, whereas (**F**) slow-burst amplitude and (**G**) the rate of sustained release pass through a transient maximum to eventually diminish. All values are given as mean ± SEM.

had a mild inhibitory effect on overall exocytosis (Fig. 2A). The inhibition profile was well described by a linear dependency on the fraction of mCh-SN25BL5**. Kinetic analysis revealed a progressive slowdown of release kinetics (Fig. 2B), owing to a gradual increase of fast- and slow-burst time constants (Fig. 2, C and D) combined with decreased amplitude of the fast component (Fig. 2E). For cells expressing low levels of mCh-SN25BL5** (0 to 20%, group I), the decrease in fast-release amplitude was partly compensated for by an increase in slow-burst amplitude (Fig. 2F) and in the rate of sustained secretion (Fig. 2G). Overall, vesicles fuse at lower rates in the presence of SN25BL5**, implying that the vesicular release probability is decreased. Because exocytosis cannot be mediated by fusion complexes solely containing SN25BL5**, this finding indicates the formation of mixed fusion complexes containing both EGFP-SN25B and mCh-SN25BL5**.

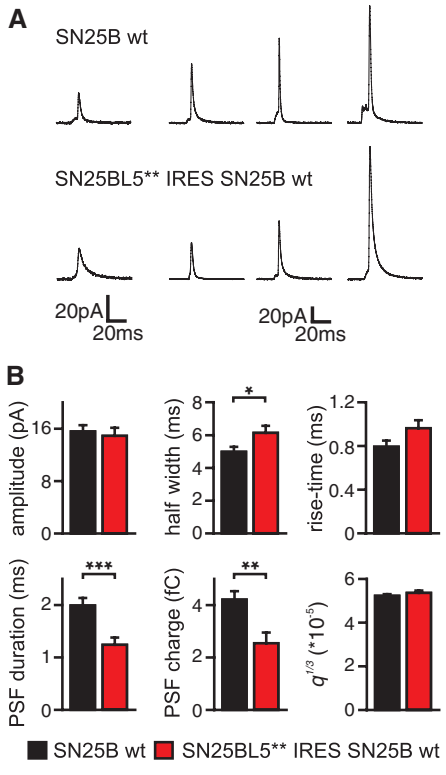

Fig. 3. Altered amperometric spikes in the presence of SN25BL5** indicate the existence of heteromeric fusion complexes. (**A**) Examples showing amperometric spikes in control cells (*Snap-25*$^{-/-}$ expressing EGFP-SN25B) and cells coexpressing WT and mutant SNAP-25B (mCh-SN25BL5**-IRES-EGFP-SN25B). (**B**) Quantitative analysis. The means of cell medians for each parameter ± SEM are shown (*q*, total charge). The half width was slightly prolonged in the presence of SN25BL5** ($P < 0.05$). The pre-spike foot duration and charge were reduced, indicating altered fusion-pore opening (**$P < 0.01$ and ***$P < 0.001$; Student's *t* test).

Formation of mixed fusion complexes was also supported by experiments examining single-vesicle fusion events (Fig. 3). In these experiments, *Snap-25*$^{-/-}$ cells were infected with a SFV expressing ~80% mCh-SN25BL5** and ~20% EGFP-SN25B (fig. S3D). In the presence of mCh-SN25BL5**, amperometric spikes exhibited a slightly delayed overall waveform and a decreased duration of pre-spike feet (PSF). Because mCh-SN25BL5** cannot support exocytosis on its own, these data indicate single-vesicle fusion using mixed complexes. A similar reduction in PSF duration has been described upon mutating the C-terminal layers of synaptobrevin-2 (*18*).

The above findings suggested that multiple SNARE complexes might surround the nascent fusion pore (*12*). Thus, we asked how many SNARE complexes are needed for fast vesicle fusion. Assuming that the incorporation of one copy of SN25BL5** is sufficient to decrease the vesicular release rate, vesicle fusion with normal fast kinetics should be mediated by complexes containing exclusively WT SN25B. The number of such vesicles depends on the fractional availability of WT SN25B raised to a power of *n*, where *n* is the number of SN25B molecules in the fusion complex (*20*). To determine the amount of fusion with unperturbed kinetics, we repeated the kinetic analysis, but this time we fixed the fast time constant τ_{fast} to the control value (EGFP-SN25B, τ_{fast} = 19.8 ms), such that the amplitude reports unperturbed secretion. The number of fast-fusing vesicles diminished much faster than overall secretion with an increasing proportion of mCh-SN25BL5** (Fig. 4A, compare with Fig. 2A). Fitting of a simple binomial model (*21*) to the entire curve identified $n = 2.8$. Alternatively, we fitted a straight line to the left part of the curve, following logarithmic transform of the burst am-

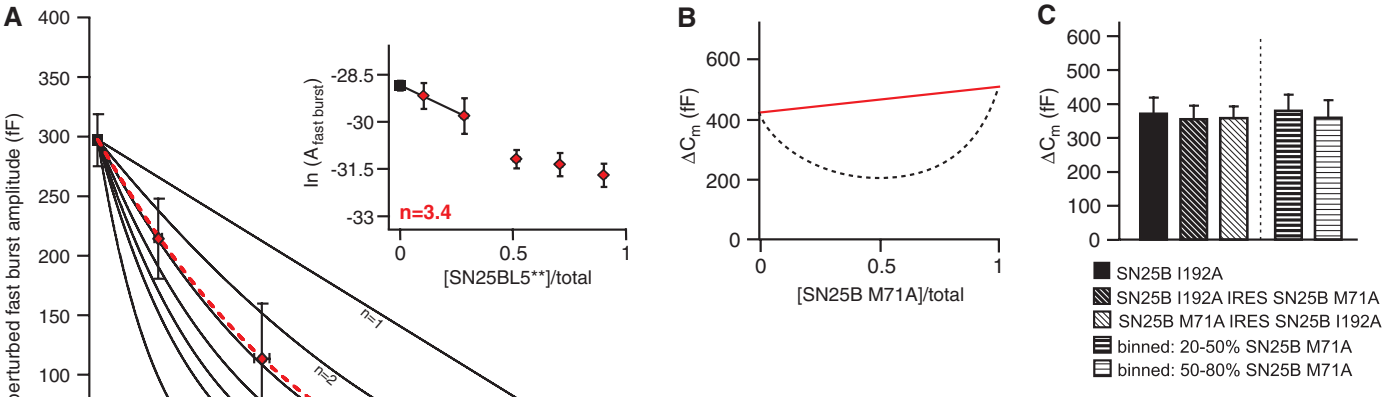

Fig. 4. Fast-fusing vesicles display higher-order dependence on the availability of SNAP-25. (**A**) Plot of unperturbed fast-burst amplitude versus SN25BL5** fraction (mean ± SEM). Fit of a binomial model (*20*) yielded $n = 2.8$ or 3.4 after the logarithmic transform, respectively (inset), interpreted as the number of SNARE complexes driving fast vesicles. The black square denotes fast-burst amplitude ($A_{fast\ burst}$), as derived for WT SN25B-expressing control cells. (**B**) If SNAP-25 cross-links SNARE complexes, coexpression of both single mutations should cause maximal inhibition at a 1:1 ratio of the two mutants (dashed line); otherwise, secretion should follow a linear interpolation line (red solid line). (**C**) Secretion was not inhibited in cells coexpressing SN25BM71A and SN25BI192A compared with reference recordings (SN25B I19A). Error bars indicate mean ± SEM. Examining data in the 20-to-50% or 50-to-80% expression bins also did not reveal any inhibition.

plitude (*21*), which yielded $n = 3.4$ (inset, Fig. 4A). Our model assumes that the affinity of SN25BL5** to the rest of the fusion apparatus is unchanged, which appears likely from previous data (*14*). Three is a lower estimate of the number of SNARE complexes in a fusion complex driving fast fusion, because incorporation of more than one mutant might be required to detectably change fusion kinetics.

SNAP-25 harbors two SNARE domains and could possibly contribute these to different SNARE complexes, thereby cross-linking them (*21*, *22*). This would separate the two single mutations and mask a dominant-negative effect of SN25BL5** in the presence of WT protein (fig. S5A), which could provide an alternative explanation for the shallow dependence of overall secretion on SN25BL5** fraction (Fig. 2A). We tested such "domain-swapping" by coexpression of the two single-layer +5 mutants (M71A and I192A). At similar expression levels, the two single alanines should recreate the catastrophic double-layer +5 mutation in half of the complexes (fig. S5B), which should result in a 50% drop in secretion (Fig. 4B, according to Fig. 2A). Using two bicistronic SFVs that express both mutants at the proportions [mCh-SN25M71A]/total of 15 ± 1% or 65 ± 3%, we observed no inhibitory effect on secretion (Fig. 4C). In addition, examining data in 20-to-50% or 50-to-80% expression bins did not identify any block of release (Fig. 4C). Thus, domain-swapping cannot explain the mild inhibition by SN25BL5**, nor can it represent a prominent event during exocytosis, consistent with the finding that separated SNAP-25 SNARE domains support in vitro vesicle fusion (*23*) and secretion (*24*).

Using a titration approach in intact cells, we report here that the apparent cooperativity for fast-phase secretion is higher (~3) than that for overall exocytosis (~1). We conclude that SNARE complexes form higher-order functional units, and at least three SNARE complexes are required for the fast phase of exocytosis (fig. S5, C and D). Our findings agree with data from infusion of synaptobrevin fragments into PC12 cells (*11*). The linear titration profile of overall secretion might be explained if stoichiometry of fusion complexes is not fixed. Vesicles resident at the plasma membrane have time to form several SNARE complexes in the absence of stimulation, achieving faster speeds of fusion when triggered by calcium. However, vesicles arriving during conditions of sustained high calcium concentrations might fuse using fewer [or possibly only a single (*8*)] SNARE complexes. The dramatic shift in release rate upon coexpression of SN25BL5** suggests that the number of functional (that is, completely zippering) SNARE complexes is a determinant of fusion probability. Indeed, variable fusion stoichiometry might underlie heterogeneity in vesicular release probabilities between synapses (*25*) or release phases (*26*) and could represent an important regulated parameter in neurotransmitter-releasing cells.

References and Notes

1. R. Jahn, R. H. Scheller, *Nat. Rev. Mol. Cell Biol.* **7**, 631 (2006).
2. R. B. Sutton, D. Fasshauer, R. Jahn, A. T. Brunger, *Nature* **395**, 347 (1998).
3. J. B. Sørensen, *Annu. Rev. Cell Dev. Biol.* **25**, 513 (2009).
4. F. Li *et al.*, *Nat. Struct. Mol. Biol.* **14**, 890 (2007).
5. K. Wiederhold, D. Fasshauer, *J. Biol. Chem.* **284**, 13143 (2009).
6. A. Yersin *et al.*, *Proc. Natl. Acad. Sci. U.S.A.* **100**, 8736 (2003).
7. W. Liu, V. Montana, V. Parpura, U. Mohideen, *Biophys. J.* **95**, 419 (2008).
8. G. van den Bogaart *et al.*, *Nat. Struct. Mol. Biol.* **17**, 358 (2010).
9. M. K. Domanska, V. Kiessling, A. Stein, D. Fasshauer, L. K. Tamm, *J. Biol. Chem.* **284**, 32158 (2009).
10. E. Karatekin *et al.*, *Proc. Natl. Acad. Sci. U.S.A.* **107**, 3517 (2010).
11. Y. Hua, R. H. Scheller, *Proc. Natl. Acad. Sci. U.S.A.* **98**, 8065 (2001).
12. C. Montecucco, G. Schiavo, S. Pantano, *Trends Biochem. Sci.* **30**, 367 (2005).
13. X. Han, C.-T. Wang, J. Bai, E. R. Chapman, M. B. Jackson, *Science* **304**, 289 (2004); published online 11 March 2004 (10.1126/science.1095801).
14. J. B. Sørensen *et al.*, *EMBO J.* **25**, 955 (2006).
15. J. B. Sørensen *et al.*, *Cell* **114**, 75 (2003).
16. Materials and methods are available as supporting material on *Science* Online.
17. H. de Wit *et al.*, *Cell* **138**, 935 (2009).
18. A. M. Walter, K. Wiederhold, D. Bruns, D. Fasshauer, J. B. Sørensen, *J. Cell Biol.* **188**, 401 (2010).
19. Y. Aikawa, K. L. Lynch, K. L. Boswell, T. F. Martin, *Mol. Biol. Cell* **17**, 2113 (2006).
20. A derivation of the rosette model of SNARE complexes is available as supporting material on *Science* Online.
21. D. H. Kweon *et al.*, *Biochemistry* **41**, 5449 (2002).
22. H. Tokumaru *et al.*, *Cell* **104**, 421 (2001).
23. F. Parlati *et al.*, *Proc. Natl. Acad. Sci. U.S.A.* **96**, 12565 (1999).
24. Y. A. Chen, S. J. Scales, S. M. Patel, Y. C. Doung, R. H. Scheller, *Cell* **97**, 165 (1999).
25. C. Rosenmund, J. D. Clements, G. L. Westbrook, *Science* **262**, 754 (1993).
26. Y. Goda, C. F. Stevens, *Proc. Natl. Acad. Sci. U.S.A.* **91**, 12942 (1994).

27. We thank I. Herfort and D. Reuter for expert technical assistance and S. Young for help with viral expression systems. This work was supported by the Lundbeck Foundation (Junior Group Leader Fellowship, J.B.S.), the Lundbeck Foundation Center for Biomembranes in Nanomedicine (J.B.S.), the Danish Medical Research Council (J.B.S.), the Netherlands Organization for Scientific Research (Pionier/VICI900-01-001 and ZonMW 903-42-095 to M.V. and VENI 916-36-043 to H.d.W.), the NeuroBsik Mouse Phenomics Consortium (BSIK03053), and the European Union Seventh Framework Programme under grant agreement no. HEALTH-F2-2009-242167 ("SynSys" project to both J.B.S. and M.V.).

Supporting Online Material

www.sciencemag.org/cgi/content/full/science.1193134/DC1
Materials and Methods
SOM Text
Figs. S1 to S5
References

2 June 2010; accepted 27 August 2010
Published online 16 September 2010;
10.1126/science.1193134
Include this information when citing this paper.

Mechanisms of Proton Conduction and Gating in Influenza M2 Proton Channels from Solid-State NMR

Fanghao Hu, Wenbin Luo, Mei Hong*

The M2 protein of influenza viruses forms an acid-activated tetrameric proton channel. We used solid-state nuclear magnetic resonance spectroscopy to determine the structure and functional dynamics of the pH-sensing and proton-selective histidine-37 in M2 bound to a cholesterol-containing virus-envelope-mimetic membrane so as to better understand the proton conduction mechanism. In the high-pH closed state, the four histidines form an edge-face π-stacked structure, preventing the formation of a hydrogen-bonded water chain to conduct protons. In the low-pH conducting state, the imidazoliums hydrogen-bond extensively with water and undergo microsecond ring reorientations with an energy barrier greater than 59 kilojoules per mole. This barrier is consistent with the temperature dependence of proton conductivity, suggesting that histidine-37 dynamically shuttles protons into the virion. We propose a proton conduction mechanism in which ring-flip–assisted imidazole deprotonation is the rate-limiting step.

Proton transport in synthetic materials is mediated either solely by hydrogen-bonded (H-bonded) water, as in hydrated ionic polymers (*1*), or solely by titratable heterocycles, such as imidazoles tethered to the backbone of anhydrous polymers (*2*). In comparison, the conduction mechanism of biological proton channels in cell membranes is more complex because both water and titratable protein sidechains are usually present (*3*). The influenza M2 protein forms a tetrameric proton channel that is important for the virus life cycle (*4*). Activated below pH 6, the M2 channel conducts 10 to 10,000 protons per second (*5*, *6*). The pH-sensing and proton-selective residue is a single histidine, His37, in the trans-

Department of Chemistry, Iowa State University, Ames, IA 50011, USA.

*To whom correspondence should be addressed. E-mail: mhong@iastate.edu